Turkish Journal of Chemistry

http://journals.tubitak.gov.tr/chem/

Research Article

Turk J Chem
(2014) 38: 825 – 836

doi:10.3906/kim-1401-73

Green synthesis of Fe_3O_4 nanoparticles by one-pot saccharide-assisted hydrothermal method

Ayşe DEMİR[1,2], **Abdulhadi BAYKAL**[1,*], **Hüseyin SÖZERİ**[3]

[1]Department of Chemistry, Faculty of Arts and Sciences, Fatih University, Büyükçekmece, İstanbul, Turkey

[2] Department of Chemistry, İstanbul Medeniyet University, Üsküdar, İstanbul, Turkey

[3]TÜBİTAK National Metrology Institute, Gebze, Kocaeli, Turkey

Received: 27.01.2014 • **Accepted:** 01.04.2014 • **Published Online:** 15.08.2014 • **Printed:** 12.09.2014

Abstract: A saccharide-assisted hydrothermal route starting from a single iron precursor was employed to study the influence of reducing saccharides on the formation of iron oxide (Fe_3O_4) nanoparticles (NPs). Fe_3O_4 NPs, which were confirmed by X-ray diffraction analysis, were successfully synthesized by a hydrothermal method in which mannose, maltose, lactose, and galactose served as reducing agents. The formation of Fe_3O_4 NPs was also confirmed by Fourier transform infrared spectroscopy. Samples exhibited different crystallite sizes estimated based on line profile fitting as 12 ± 2, 9 ± 2, 13 ± 3, and 9 ± 3 nm for mannose, maltose, lactose, and galactose, respectively. Magnetic characterization results revealed superparamagnetic features of the NPs obtained with galactose, mannose, and maltose.

Key words: Magnetic nanomaterials, Fe_3O_4, green synthesis, sugars, magnetic properties

1. Introduction

Magnetic nanoparticles (MNPs) have attracted considerable interest in recent years due to their unusual properties different from their bulk counterparts. MNPs have a high specific surface area that can be utilized for many applications in microwave absorption,[1] rechargeable batteries,[2] electrodes, sensors,[3,4] and electromagnetic interface (EMI) shielding.[5] Magnetite (Fe_3O_4) is one of the most important materials and it has been recently studied among MNPs owing to its unique chemical and physical properties such as superparamagnetism, high coercivity, low Curie temperature, and high magnetic susceptibility.[6–10] Since control of the chemical, physical, and magnetic properties is essential to tailor the size, shape, and morphology of Fe_3O_4 NPs, many scientists have been trying to develop a simple and efficient process to obtain Fe_3O_4 NPs with the desired characteristics.

There have been various chemical methods applied to produce superparamagnetic Fe_3O_4 NPs, such as hydrothermal synthesis, thermal decomposition,[11,12] gel-to-crystalline conversion,[13] the sol-gel method,[14] and the reduction of hematite by CO.[15] The most common method involves the use of an excess of reducing agents such as $NaBH_4$,[16] sodium citrate,[17] hydrazine,[18] carbon monoxide (CO),[19] and dimethylformamide (DMF)[20] to co-precipitate ferrous (Fe^{+2}) and ferric (Fe^{+3}) ions. However, all of these chemicals have contaminants and waste products harmful to the environment. Hence, it is very important to develop a facile and green method to fabricate superparamagnetic Fe_3O_4 NPs.

In recent years, although green chemistry and chemical processes have been developed in nanoscience

*Correspondence: hbaykal@fatih.edu.tr

and nanotechnology as well as classical wet-chemistry routes for the fabrication of NPs, they are not very widespread. The green methods for the production of NPs involve naturally occurring reagents such as vitamins, saccharides, plant extracts, biodegradable polymers, and microorganisms as reductants and capping agents.[21] The utilization of saccharides in this approach has its own several distinct features. Saccharides are easily available for use as reducing agents. In addition, they are cheap and ecofriendly. Furthermore, upon their utilization, it is not necessary to use any stabilizing agents or capping agents.[22] Lartigue et al.[23] synthesized water-soluble biocompatible rhamnose-coated Fe_3O_4 NPs of 4.0 nm via the organic phase covalent anchorage of acetate-protected rhamnose on the NPs. In comparison to the previously published NPs coated with other saccharide molecules,[24–27] the present NPs are monodispersed and size controlled and show good stability due to the covalent anchorage of rhamnose to the surface of the NPs. They present superparamagnetic behavior and nuclear relaxivities comparable with those of Endorem.

Superparamagnetism (nothing but an ensemble of NPs, in which the interparticle magnetic interactions are sufficiently weak. When the interparticle interactions are nonnegligible, the system eventually shows collective behavior, which overcomes the individual anisotropy properties of the particles) is a form of magnetism that appears in small ferromagnetic or ferrimagnetic NPs. In small enough NPs, magnetization can randomly flip direction under the influence of temperature. In the absence of an external magnetic field, when the time used to measure the magnetization of the NPs is much longer than the Néel relaxation time (time between 2 flips), their magnetization appears to be on average zero; they are said to be in the superparamagnetic state. In this state, an external magnetic field is able to magnetize the NPs, similarly to a paramagnet. However, their magnetic susceptibility is much larger than that of paramagnets.[28,29]

In this paper, we report a facile and green method for the synthesis of superparamagnetic Fe_3O_4 NPs using commonly available saccharides as reducing agents. We compared the effect of 5 different saccharides as reducing agents on the sizes for superparamagnetic Fe_3O_4.

2. Results and discussion

2.1. XRD analysis

The XRD powder diffraction patterns of Fe_3O_4 NPs synthesized with different saccharides are presented in Figure 1, which shows that all of the observed diffraction peaks belong to Fe_3O_4 and they can be indexed by the cubic structure of Fe_3O_4 (JCPDS no. 19–629), revealing a high phase purity of the product, and the diffraction peaks are broadened owing to very small crystallite size. The mean size of the crystallites was estimated from the diffraction pattern by line profile fitting method using the equation given below.[30,31] The line profile, shown in Figure 1, was fitted for 5 observed peaks with the following Miller indices: (220), (311), (400), (511), and (440). In the XRD powder pattern of the product, no other iron oxide peaks were observed. The average crystallite sizes of the product obtained as a result of this line profile fitting are tabulated in the Table. It is important to note that fructose did not lead to the formation of MNPs.

$$< LP\left(q;< R >,\sigma\right) \geq = \frac{< R >^3}{\sqrt{2\pi}\, q^4\sigma^6 \left(1+\frac{q^2\sigma^4}{<R>^2}\right)^{\frac{<R>^2}{2\sigma^2}} \left(\frac{<R>^2}{\sigma^2-1}\right)\left(\frac{<R>^2}{\sigma^2-2}\right)\left(\frac{<R>^2}{\sigma^2-3}\right)}$$

$$x\left\{3\left(1+\frac{q^2\sigma^4}{< R >^2}\right)^{<\frac{R>^2}{2\sigma^2}} \left(2+\frac{q^2\sigma^4}{< R >^2}\left(\frac{< R >^2}{\sigma^2}-2\right)\left(\frac{< R >^2}{\sigma^2}-3\right)\right)\right\}$$

$$-6\left(1+\frac{q^2\sigma^4}{\langle R\rangle^2}\right)^{\frac{3}{2}}\cos\left[\left(\frac{\langle R\rangle^2}{\sigma^2}-3\right)\tan^{-1}\left(\frac{q\sigma^2}{\langle R\rangle}\right)\right]$$

$$-6\frac{q\sigma^2}{\langle R\rangle}\left(1+\frac{q^2\sigma^4}{\langle R\rangle^2}\right)\left(\frac{\langle R\rangle^2}{\sigma^2}-3\right)\sin\left[\left(\frac{\langle R\rangle^2}{\sigma^2}-2\right)\tan^{-1}\left(\frac{q\sigma^2}{\langle R\rangle}\right)\right],$$

where q is the scattering vector, $< R >$ is the average grain size, and σ is the standard deviation of the grain size.

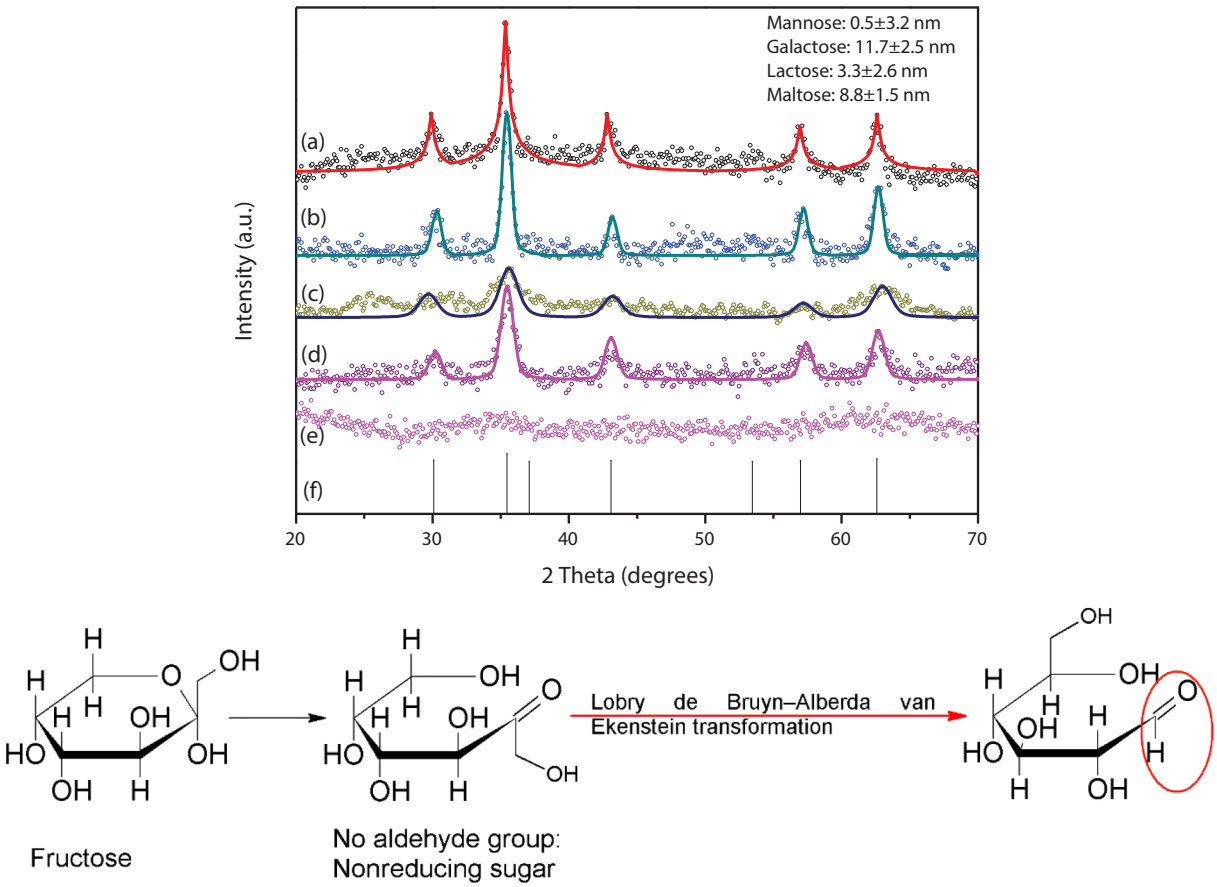

Figure 1. (a) XRD powder patterns of the products obtained for the green synthesis of Fe_3O_4 NPs with (a) mannose, (b) galactose, (c) lactose, (d) maltose, (e) fructose, and (f) the standard pattern of the magnetite (AMCSD card no. 99-100-7120) with line profile fitting. (b) The Lobry de Bruyn–Alberda van Ekenstein transformation of fructose.

Table. Average particle size, crystallite size, magnetization value, and percent inorganic/organic content of Fe_3O_4 NPs prepared in the presence of different saccharides.

	Particle size from TEM (nm)	Crystallite size from XRD (nm)	Ms (emu/g)	% Inorganic content	% Organic content
Mannose	13.1 ± 0.3	12.4 ± 2.1	59.1	75	25
Maltose	9.7 ± 0.99	9.1 ± 1.5	37.4	51	49
Lactose	3.8 ± 0.21	2.9 ± 1.4	22.02	48	52
Galactose	12.4 ± 0.3	11.9 ± 1.8	58.08	73	27
Fructose	-	-	-	-	-

As stated by Kenouche et al.[32] the saccharide motif provides good biocompatibility and biodistribution in a physiological medium, and saccharides are used as reductants that are mild, renewable, inexpensive, and nontoxic without any additional stabilizer and dispersant.[33] No purgation or protection procedure is necessary; this simple approach allows the synthesis of magnetite NPs to be extended into the industrial range with mass production.[34]

The sugars that can reduce Tollen's reagent and Fehling's solution are known as reducing sugars. They contain a free aldehydic or ketonic group along with a hydroxyl (OH) group on the carbon adjacent to these groups. However, fructose can be a reducing sugar after the following transformation.[35,36]

2.2. FT-IR analysis

FT-IR spectra of the products for the green synthesis of Fe_3O_4 NPs with mannose, maltose, lactose, galactose, and fructose are displayed in Figures 2a to 2e, respectively. The presence of stretching at 1404 cm^{-1} proved that the carboxylate group is bound to the surface of magnetite symmetrically. The values of the peaks at 2920 cm^{-1} and 2852 cm^{-1} were proposed for the asymmetrical $\nu_{as}(CH_2)$ and symmetrical $\nu_s(CH_2)$ C–H stretching regions, respectively.[37] It is known that 2 binding modes have been suggested for surface carboxylate bonding.[38–41] In one mode, the carboxylate group binds symmetrically to the surface and the symmetrical C=O stretching band should appear at 1404 cm^{-1}. In the other mode, both symmetrical C=O (1440 cm^{-1}) and asymmetrical (1552 cm^{-1}) stretching were observed.[18–20] The first type of binding is presented in Figure 2. Therefore, it is suggested that the carboxylate group in this study might bind to the magnetite surface symmetrically.

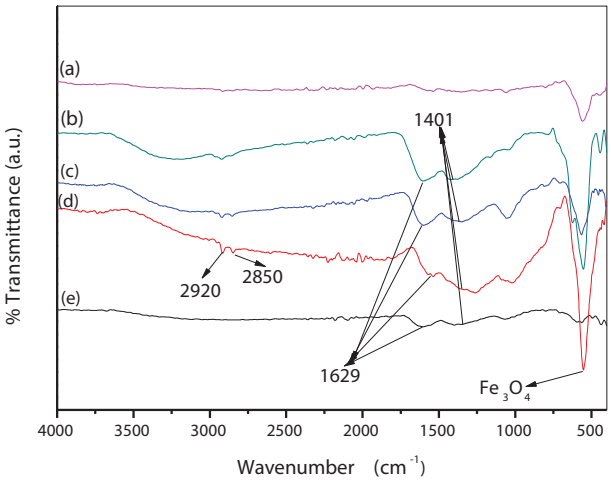

Figure 2. FT-IR spectra of the products obtained for the green synthesis of Fe_3O_4 NPs with (a) mannose, (b) maltose, (c) lactose, (d) galactose, and (e) fructose.

2.3. TEM analysis

TEM images of SPION synthesized with different saccharides and their size distribution histograms obtained from the TEM micrographs are presented in Figures 3 and 4, respectively. Particles are observed to have a mixture of spherical-like, rod-like, and dendritic nanostructure with some extent of agglomeration. However, the TEM images of the particles prepared in the presence of fructose are highly agglomerated and do not

have a cubic morphology. The procedure with fructose did not produce MNPs due to the nonreducing feature of fructose. The average sizes of the NPs synthesized with different saccharides were calculated by counting ∼100 particles by using different TEM images. The sizes estimated from the TEM micrographs are in good agreement with the crystallite sizes estimated from the XRD line profile fitting, which may reveal the nearly single crystalline character of Fe_3O_4 NPs. The calculated particle sizes of the products are tabulated in the Table.

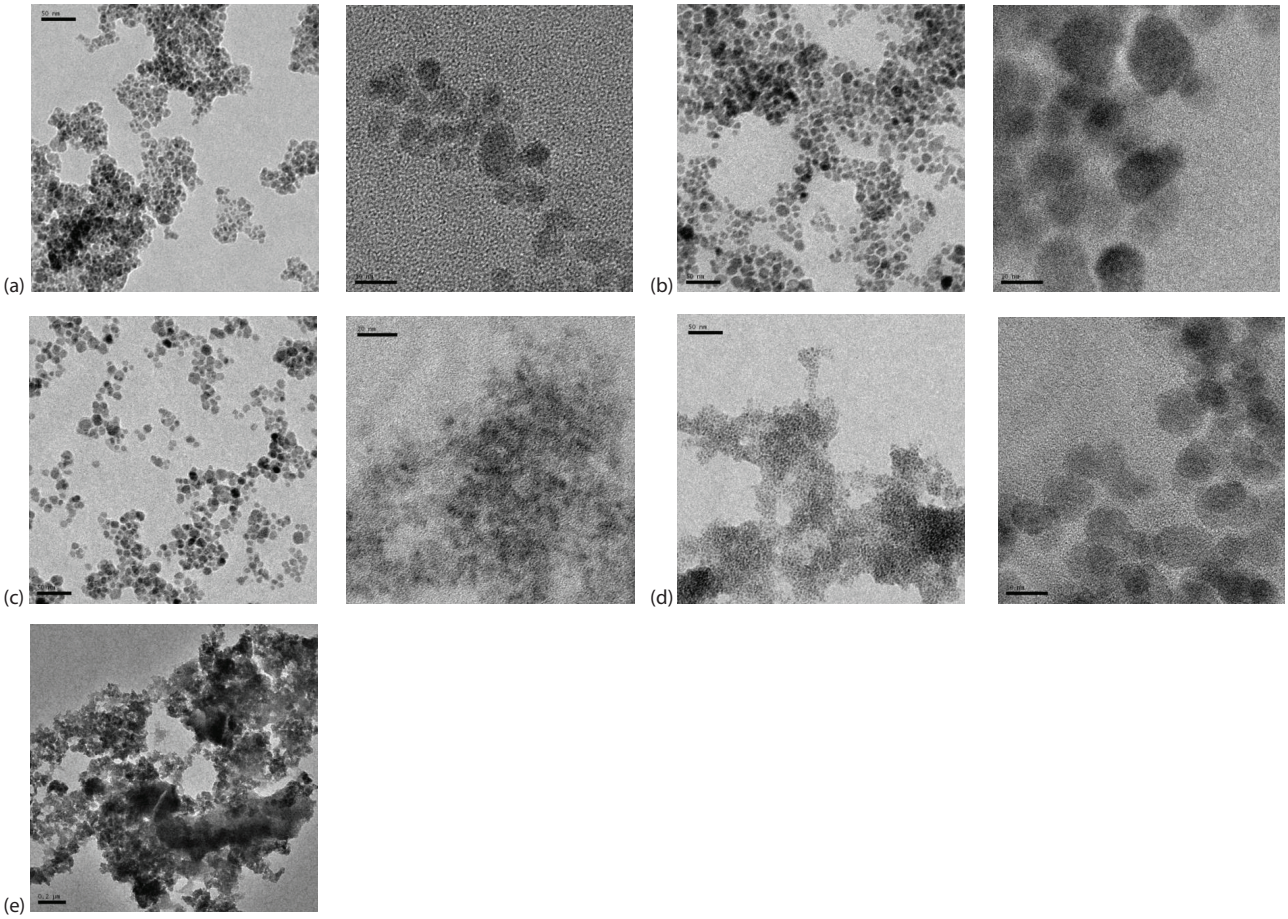

Figure 3. TEM images of the particles obtained for the synthesis of Fe_3O_4 in the presence of (a) maltose, (b) mannose, (c) galactose, (d) lactose, and (e) fructose.

2.4. Thermal analysis

TGA measurements can reveal the percentage of a coating agent on the surface of Fe_3O_4 NPs that could prevent the agglomeration of the particles due to the steric hindrance present among them. TG thermograms for the green synthesis of Fe_3O_4 NPs assisted by mannose, galactose, fructose, lactose, and maltose are presented in Figure 5 and the percent organic and inorganic content of the products are tabulated in the Table. There are 2 weight-loss processes in each TGA curve: the initial one as a result of the dehydration of the samples and the second one due to the evaporation and the desorption of the coating agents (including corresponding saccharides and gluconic acid).[41] As stated by Sun et al., particles with smaller size have a larger surface area

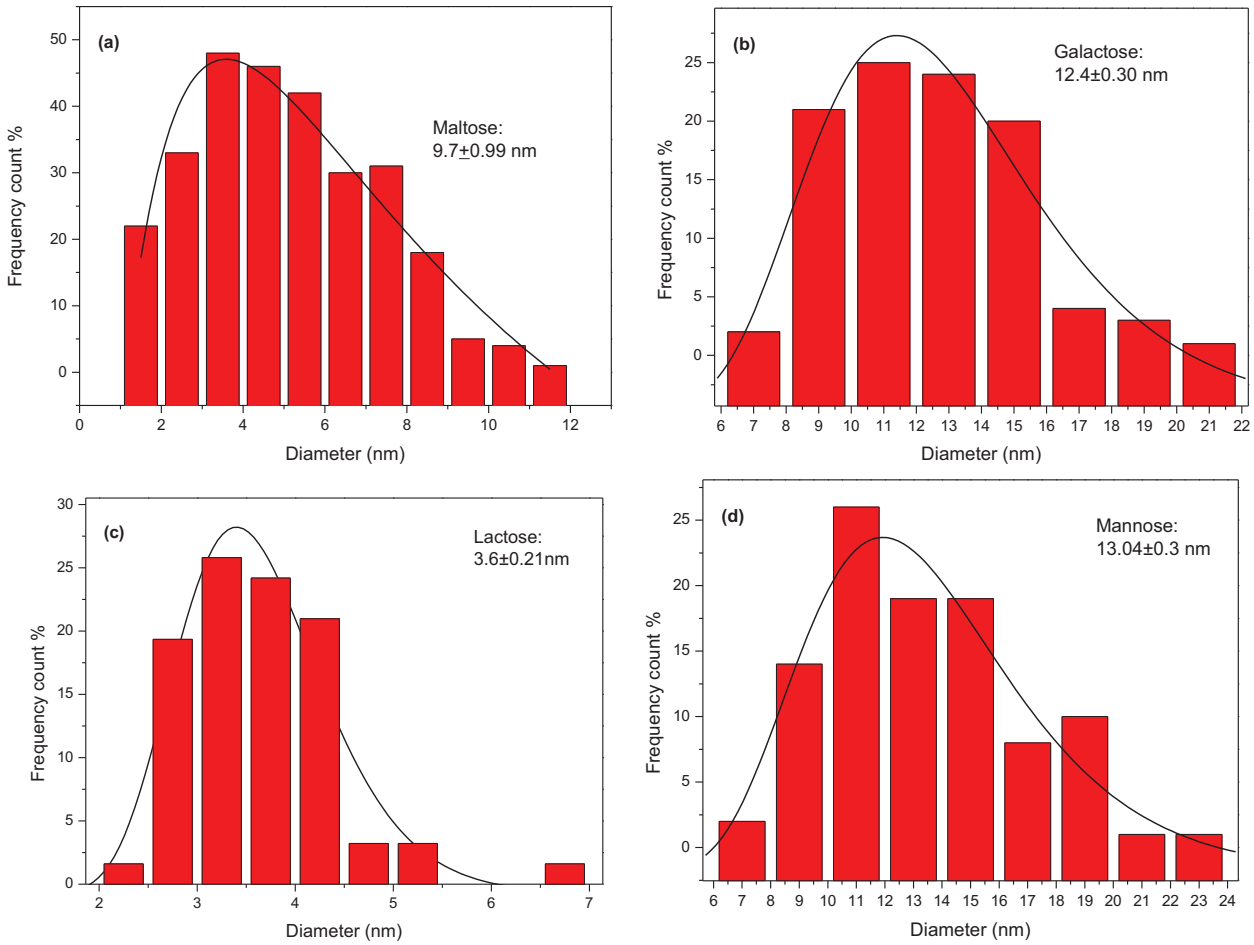

Figure 4. Particle size distribution diagrams calculated from TEM images of the Fe_3O_4 NPs prepared with (a) maltose, (b) galactose, (c) lactose, and (d) mannose.

that can adsorb a larger amount of coating agents on the particle surface, and vice versa.[34] The Fe_3O_4 NP system synthesized with the assistance of maltose and lactose has the smallest crystallite size as well as the size calculated from TEM images, while the highest weight loss is also observed for these carbohydrates, which are both disaccharides. As a result, the small size leads to the formation of a thicker coating on the surface of the NPs. Moreover, since both maltose and lactose are disaccharides each containing a glucose unit, they are initially hydrolyzed into their corresponding reducing monosaccharides: 2 equivalents of glucose for maltose and 1 equivalent from both galactose and glucose for lactose. Then these monosaccharides are oxidized to their acidic forms such as gluconic acid. Each equivalent of disaccharides yields 2 equivalents of monosaccharides, while mannose and galactose only yield 1 equivalent. This, in turn, causes the Fe_3O_4 NPs synthesized by monosaccharides to be larger and have a thinner coating and the ones prepared with disaccharides to be smaller and yet have a thicker surface coating.

2.5. Magnetization measurements

Room temperature M–H hysteresis curves of magnetite NPs synthesized with different saccharide types are shown in Figures 6a–6e. Samples prepared with galactose, mannose, and maltose have superparamagnetic

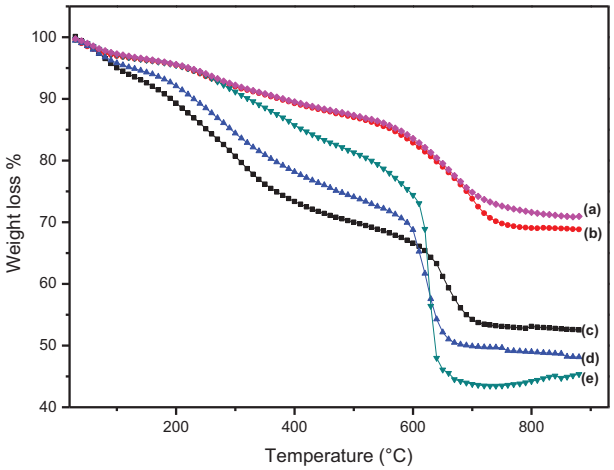

Figure 5. TG thermograms of the products obtained for the green synthesis of Fe_3O_4 NPs with (a) mannose, (b) galactose, (c) fructose, (d) lactose, and (e) maltose.

features, namely unsaturated magnetization and the absence of coercivity. However, saturation magnetization values of these samples are different in such a way that the specimens with galactose and mannose have higher saturation magnetization values (Ms $\sim$ 60 emu/g) compared to those of the sample prepared in the presence of maltose (Ms $\sim$ 40 emu/g). According to the XRD patterns shown in Figure 1, the crystallinity is better in samples prepared with the assistance of galactose and mannose, and so the magnetization is higher. In the sample prepared with fructose, the target phase (i.e. magnetite) was not formed at all, and thus the magnetization was very weak even at high fields. The small fraction of the magnetite phase in the sample prepared with lactose along with its lower crystallinity resulted in a weaker magnetization (Ms = 20 emu/g) at high fields yet again. As a result, the magnetization measurements reveal that the reducing agents mannose and galactose promote the phase formation of magnetite. Even for these samples, the magnetization is smaller than that of the bulk particles, which is around 92 emu/g.[42] This reduced magnetization is another feature of superparamagnetic NPs and can be explained by the surface spin disorder and spin canting effects,[43,44] which occur when the surface to volume ratio of particles increases while the particle size decreases. The magnetic behavior of superparamagnetic NPs can be described by Langevin function, which is used to fit the experimental M–H hysteresis curves to calculate the mean magnetic moment of particles: $\mu = M_s \pi \rho D^3/6$. Thus, it is possible to get the average diameter (D) of NPs by using the experimentally determined Ms value and the density of the magnetite (ρ = 5.18 g/cm^3). Hence, we obtained the mean magnetic moment of particles as 14.909 μ_B and the average diameter as 9.6 nm, which are close to the values derived from XRD patterns. Figure 6 inset shows Langevin fit of the measured M–H hysteresis curve of NPs synthesized in the presence of galactose.

3. Conclusion

A simple, ecofriendly and economical, single- and inexpensive-precursor-based hydrothermal approach assisted by mannose, galactose, fructose, maltose, and lactose was used to synthesize Fe_3O_4 NPs. The particle size of the Fe_3O_4 NPs synthesized with different saccharides varied from 3.8 to 13.1 nm. Except for fructose, all saccharides acted as bifunctional agents: both as the precursor of the reducing agent to make the formation of the magnetite phase only from the Fe (III) precursor, $FeCl_3$, and as the source of the coating agent to

form small Fe_3O_4 NPs by preventing particle growth and agglomeration. The procedure did not result in the expected product when fructose–a nonreducing monosaccharide–was employed. The coated Fe_3O_4 NPs have potential biotechnological and biomedical applications as well as potential use in magnetic resonance imaging and catalysis. Moreover, since there is no need to protect the reaction environment by an inert gas, this simple technique can be applied to obtain Fe_3O_4 NPs in the industrial range with mass production.

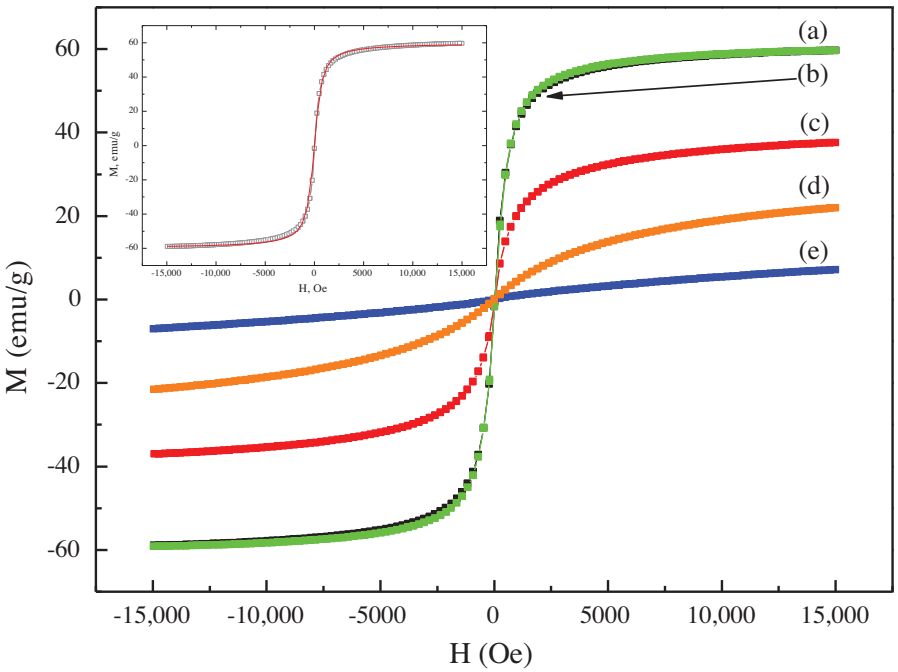

Figure 6. Room temperature M–H curves of the particles obtained for the green synthesis of Fe_3O_4 NPs with (a) mannose, (b) galactose, (c) maltose, (d) lactose, and (e) fructose.

4. Experimental

4.1. Materials

All chemicals were of analytical grade and were used without further purification. Ferric chloride hexahydrate ($FeCl_3.6H_2O$), α-D-maltose, α-D-mannose, α-D-galactose, α-D-fructose, α-D-lactose, and $NH_3 \cdot H_2O$ were all purchased from Fluka.

4.2. Characterization

X-ray powder diffraction (XRD) analysis was conducted on a Rigaku Smart Lab Diffractometer operated at 40 kV and 35 mA using Cu K_α radiation.

High resolution transmission electron microscopy (HR-TEM) analysis was performed using a JEOL JEM 2100 microscope. A drop of diluted sample in alcohol was dripped on a TEM grid.

Fourier transform infrared (FT-IR) spectra were recorded in transmission mode with a PerkinElmer BX FT-IR infrared spectrometer. The powder samples were ground with KBr and compressed into a pellet. FT-IR spectra in the range 4000–400 cm^{-1} were recorded in order to investigate the nature of the chemical bonds formed.

The thermal stability was determined by thermogravimetric analysis (TGA, PerkinElmer Instruments model, STA 6000). The TGA thermograms were recorded for 5 mg of powder sample at a heating rate of 10 °C/min in the temperature range of 30–800 °C under nitrogen atmosphere.

VSM measurements were performed using a vibrating sample magnetometer (LDJ Electronics Inc., Model 9600). The magnetization measurements were carried out in an external field up to 15 kOe at room temperature.

4.3. Synthesis of Fe_3O_4 magnetic NPs

An appropriate amount of mannose was dissolved in 50 mL of deionized water followed by the addition of 0.9 g of ferric chloride under vigorous stirring (saccharide to $FeCl_3$ molar ratio was 3:1). Then concentrated ammonia was added to the solution until the pH reached ~10. After 30 min, the mixture was transferred into a Teflon-lined stainless steel autoclave and sealed; afterwards it was heated to 180 °C and kept at this temperature for 48 h (Scheme c). The mixture then was cooled to room temperature and the product was collected by using a permanent magnet, washed 3 times with deionized water, and dried under vacuum at 60 °C overnight. Other MNPs were prepared by using the same procedure except that the mannose was replaced with maltose, lactose, or galactose. Another experiment when fructose was used as a negative control was also performed. The proposed reduction mechanism of the reaction and the synthesis of Fe_3O_4 NPs are summarized and the experimental set-up is illustrated in Scheme.

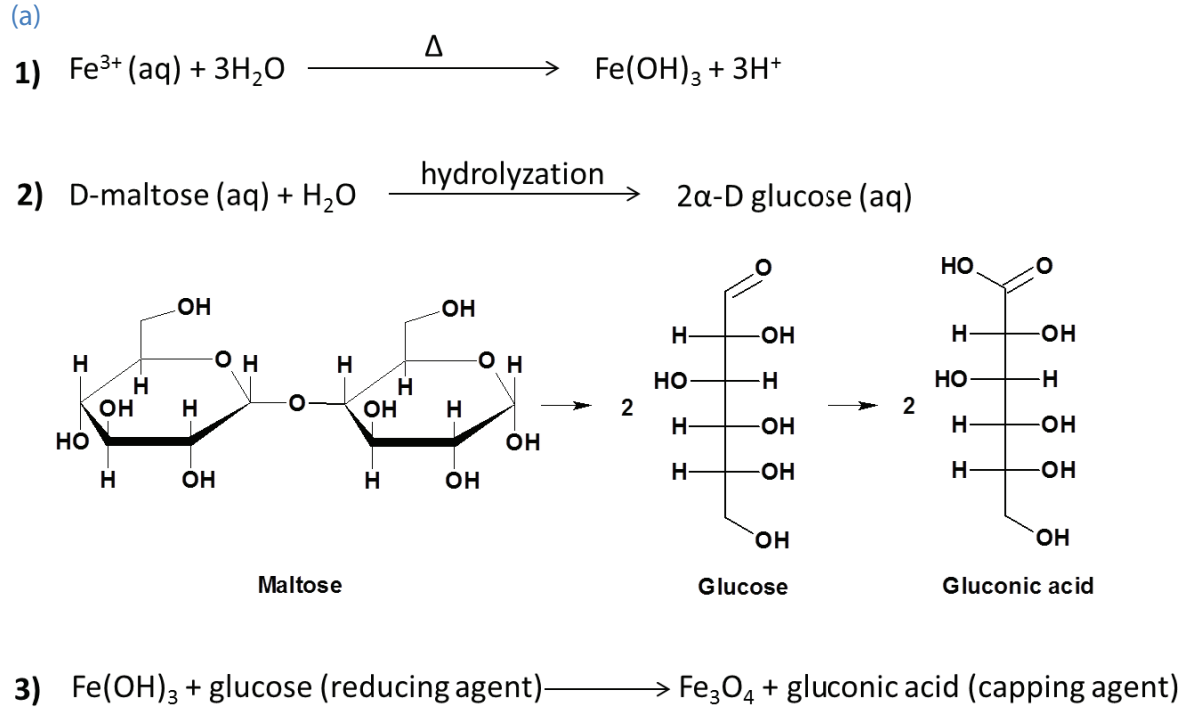

Scheme. Preparation steps for fabricating superparamagnetic Fe_3O_4 NPs: (a) proposed reactions for the synthesis of Fe_3O_4 NPs,

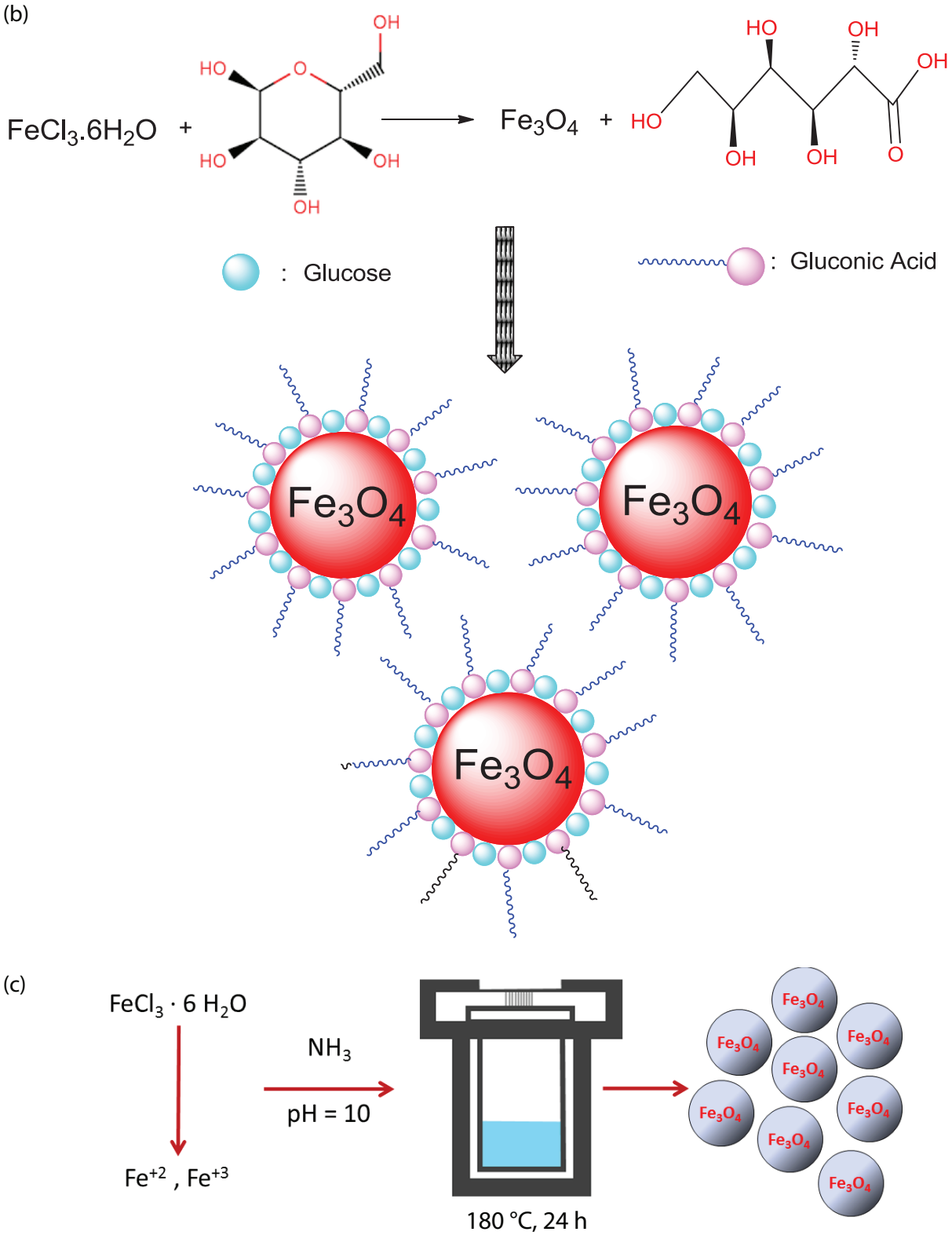

Scheme. Preparation steps for fabricating superparamagnetic Fe_3O_4 NPs: (b) illustrative scheme of the formation of Fe_3O_4 NPs, (c) experimental set-up for synthesizing Fe_3O_4 NPs.

Acknowledgment

This work is supported by the Scientific Research Fund of Fatih University under the project number P50021203-Y (2282).

References

1. He, Z.; Fang, Y.; Wang, X.; Pang, H. *Synth. Met.* **2011**, *161*, 420–425.
2. Gómez, H.; Ram, M. K.; Alvi, F.; Villalba, P.; Stefanakos, E.; Kumar, A. *J. Power Sources* **2011**, *196*, 4102–4108.
3. Rajesh, T.; Ahuja, D.; Kumar, D. *Sens. Actuators B* **2009**, *136*, 275–286.
4. Jafarzadeh, S.; Adhikari, A.; Sundall, P. E.; Pan, J. *Prog. Org. Coat.* **2011**, *70*, 108–115.
5. Lu, X.; Zhang, W.; Wang, C.; Wen, T. C.; Wei, Y. *Prog. Polym. Sci.* **2011**, *36*, 671–712.
6. Karaoğlu, E.; Baykal, A.; Deligöz, H.; Şenel, M.; Sözeri, H.; Toprak, M. S. *J. Alloys Compd.* **2011**, *509*, 8460–8468.
7. Karaoglu, E.; Baykal, A.; Erdemi, H.; Alpsoy, L.; Sozeri, H. *J. Alloys Compd.* **2011**, *509*, 9218–9225.
8. Temizel, E.; Ayan, E.; Senel, M.; Erdemi, H.; Yavuz, M. S.; Kavas, H.; Baykal, A.; Öztürk, R. *Mater. Chem. Phys.* **2011**, *131*, 284–291.
9. Karaoglu, E.; Kavas, H.; Baykal, A.; Toprak, M. S.; Sözeri, H. *Nano-Micro Lett.* **2011**, *3*, 79–85.
10. Kemikli, N.; Kavas, H.; Kazan, S.; Baykal, A.; Ozturk, R. *J. Alloys Compd.* **2010**, *502*, 439–444.
11. Si, F.; Li, C. H.; Wang, X.; Yu, D.; Peng, Q.; Li, Y. D. *Cryst. Growth Des.* **2005**, *5*, 391–393.
12. Sun, S. H.; Zeng, H. *J. Am. Chem. Soc.* **2002**, *124*, 8204–8205.
13. Özkaya, T.; Toprak, M. S.; Baykal, A.; Kavas, H.; Köseoğlu, Y.; Aktaş, B. *J. Alloys Compd.* **2009**, *472*, 18–23.
14. Tang, N. J.; Zhong, W.; Jiang, H. Y.; Wu, X. L.; Liu, W.; Du, Y. W. *J. Magn. Magn. Mater.* **2004**, *282*, 92–95.
15. Wang, P.; Lee, C.; Young, T. *J. Polym. Sci., Part A: Polym. Chem.* **2005**, *43*, 1342–1356.
16. Cain, J. L.; Harrison, S. R.; Nikles, J. A.; Nikles, D. E. *J. Magn. Magn. Mater.* **1996**, *155*, 67–69.
17. Qian, Y.; Wang, C.; Le, Z. G., *Appl. Surf. Sci.* **2011**, *257*, 10758–10762.
18. Hou, Y. L.; Hiroshi, K.; Masatsugu, S.; Erika, O. S.; Noriaiki, O.; Toshihiro, K.; Toshiaki, O. *J. Phys. Chem. B.* **2005**, *109*, 4845–4852.
19. Mondal, K.; Lorethova, H.; Hippo, E.; Wiltowski, T.; Lalvani, S. B. *Fuel Process. Technol.* **2004**, *86*, 33–47.
20. Jian, P.; Yahui, H.; Yang, W.; Linlin, L. *J. Membr. Sci.* **2006**, *284*, 9–16.
21. Kharissova, O. V.; Dias, H. V. R.; Kharisov, B. I.; Pérez, B. O.; Pérez, V. M. J. *Trends Biotechnol.* **2013**, *31*, 240–248.
22. Panigrahi, S.; Kundu, S.; Kumar, S.; Nath, S.; Pal, T. *Colloids Surf. A* **2005**, *264*, 133–138.
23. Lartigue, L.; Oumzil, K.; Guari, Y.; Larionova, Guérin, J. C.; Montero, J. L.; Montero, V. B.; Sangregorio, C.; Caneschi, A.; Innocenti, C.; et al. *Org. Lett.* **2009**, *11*, 2992–2995.
24. Shimomura, M.; Ono, B.; Oshima, K.; Miyauchi, S. *Polymer* **2006**, *47*, 5785–5790.
25. El-Boubbou, K.; Gruden, C.; Huang, X. *J. Am. Chem. Soc.* **2007**, *129*, 13392–13393.
26. Astete, C. E.; Kumar, C. S. S. R.; Sabilov, C. M. *Coll., Surf. A: Physicochem. Eng. Aspects* **2007**, *299*, 209–216.
27. Horac, D.; Babic, M.; Jendelova, P.; Herynek, V.; Trchova, M.; Pientka, Z.; Pollert, E.; Sykova, E. *Bioconjugate Chem.* **2007**, *18*, 635–644.
28. Gittleman, J. I.; Abeles, B.; Bozowski, S. *Physical Review B* **1974**, *9*, 3891–3897.
29. Kumar, A.; Tandon, R. P.; Awana, V. P. S. *J. Magn. Magn. Mater* **2014**, *349*, 224–231.
30. Wejrzanowski, T.; Pielaszek, R.; Opalinska, A.; Matysiak, H.; Łojkowski, W.; Kurzydłowski, K. J. *Appl. Surf. Sci.* **2006**, *253*, 204–208.

31. Pielaszek, R. Analytical expression for diffraction line profile for polydispersive powders, Appl. Crystallography, Proceedings of the XIX Conference, Krakow, Poland, 2003, 43–50.
32. Kenouche, S.; Larionova, J.; Bezzi, N.; Guari, Y.; Bertin, N.; Zanca, M.; Lartigue, L.; Cieslak, M.; Godin, C.; Morrot, G. *Powder Technology* **2014**, *255*, 60–65.
33. Lu, W.; Shen, Y.; Xie, A.; Zhang, W. *J. Magn. Magn. Mater* **2010**, *322*, 1828–1933.
34. Sun, X.; Zheng, C.; Zhang, F.; Yang, Y.; Wu, G.; Yu, A.; Guan, N. *J. Phys. Chem. C* **2009**, *113*, 16002–16006.
35. Angyal, S. J. In *Glycoscience: Epimerisation, Isomerisation and Rearrangement Reactions of Carbohydrates*, Vol. 215; Stütz, A. E., Ed. Springer-Verlag: Berlin, Germany, 2001, pp. 1–14.
36. Daniel J.; Reducing sugar structure, http://www.cfs.purdue.edu/fn/fn453/pdf_full/Reducing_sugar_structure.pdf (Accessed on April 30, 2014).
37. Shafi, K. V. P. M.; Ulman, A.; Yan, X.; Yang, N. L.; Estournès, C.; White, H.; Rafailovich, M. *Langmuir* **2001**, *17*, 5093–5097.
38. Tao, Y. T. *J. Am. Chem. Soc.* **1993**, *115*, 4350–4358.
39. Xuan, S.; Hao, L.; Jiang, W.; Gong, X.; Hu, Y.; Chen, Z. *J. Magn. Magn. Mater.* **2007**, *308*, 210–213.
40. Zhang, L.; He, R.; Gu, H. C. *Appl. Surf. Sci.* **2006**, *253*, 2611–2617.
41. Demir, A.; Topkaya, R.; Baykal, A. *Polyhedron* **2013**, *65*, 282–287.
42. Zhang, M.; Zhang, Q.; Itoh, T.; Abe, M. *IEEE Trans. Magn.* **1994**, *30*, 4692–4694.
43. Kodama, R. H.; Berkowitz, A. E.; McNiff, E. J.; Foner, S. *Phys. Rev. Lett.* **1996**, *77*, 394–397.
44. Batlle, X.; Labarta, A. *J. Phys. D: Appl. Phys.* **2002**, *35*, R15–R42.